Published in final edited form as:
NMR Biomed. 2015 February ; 28(2): 200–209. doi:10.1002/nbm.3243.

Imaging of Amide Proton Transfer and Nuclear Overhauser Enhancement in Ischemic Stroke with Corrections for Competing Effects

Hua Li[a,b], **Zhongliang Zu**[a,c], **Moritz Zaiss**[d], **Imad S. Khan**[e], **Robert Singer**[e], **Daniel F. Gochberg**[a,b,c], **Peter Bachert**[d], **John C. Gore**[a,b,c,f,g], and **Junzhong Xu**[a,b,c,*]

[a]Institute of Imaging Science, Vanderbilt University, Nashville, TN 37232, USA

[b]Department of Physics and Astronomy, Vanderbilt University, Nashville, TN 37232, USA

[c]Department of Radiology and Radiological Sciences, Vanderbilt University, Nashville, TN 37232, USA

[d]Department of Medical Physics in Radiology, Deutsches Krebsforschungszentrum (DKFZ, German Cancer Research Center), Im Neuenheimer Feld 280, D-69120 Heidelberg, Germany

[e]Section of Neurosurgery, Geisel School of Medicine at Dartmouth, Lebanon, NH 03756, USA

[f]Department of Biomedical Engineering, Vanderbilt University, Nashville, TN 37232, USA

[g]Department of Molecular Physiology and Biophysics, Vanderbilt University, Nashville, TN 37232, USA

Abstract

Chemical exchange saturation transfer (CEST) potentially provides the ability to detect small solute pools through indirect measurements of attenuated water signals. However, CEST effects may be diluted by various competing effects such as non-specific magnetization transfer (MT) and asymmetric MT effects, water longitudinal relaxation (T_1), and direct water saturation (RF spillover). In the current study, CEST images were acquired in rats following ischemic stroke and analyzed by comparing the reciprocals of the CEST signals at three different saturation offsets. This combined approach corrects the above competing effects and provides a more robust signal metric sensitive specifically to proton exchange rate constant. The corrected amide proton transfer (APT) data show greater differences between the ischemic and the contralateral (non-ischemic) hemispheres. By contrast, corrected nuclear Overhauser enhancements (NOEs) around −3.5 ppm from water change over time in both hemispheres, indicating whole-brain changes that have not been reported before. This study may help better understand the contrast mechanisms of APT and NOE imaging in ischemic stroke, and also establishes a framework for future stroke measurements using CEST imaging with spillover-, MT- and T_1-corrections.

[*]**Corresponding author**: Vanderbilt University Institute of Imaging Science, 1161 21st Avenue South, AA 1105 MCN, Nashville, TN 37232-2310, USA. Tel.: + 1 615 322 8359; Fax: + 1 615 322 0734. junzhong.xu@vanderbilt.edu (J. Xu).

Keywords

CEST; APT; NOE; stroke; ischemia; AREX

Introduction

Chemical exchange saturation transfer (CEST) allows the detection of relatively small solute pools by exploiting the chemical exchange between protons in the solute and free water (1,2). During CEST experiments, the exchangeable solute protons are saturated by a frequency selective radiofrequency pulse and then detected through indirect measurement of the attenuated water signals. Water signals ($S\Omega$) are usually acquired over a range of irradiation offsets (Ω) around the water resonance frequency and then normalized by the corresponding unsaturated signal (S_0). The *z*-spectrum ($Z\Omega$) = $S\Omega)/S_0$) allows the solute resonance frequency to be identified and the CEST contrast at each offset to be quantified.

Amide proton transfer (APT) imaging is a specific application of CEST in which the contrast originates from (mainly) backbone amide protons associated with mobile proteins and peptides (3–9). During acute stroke, APT reportedly shows significant differences between the ischemic and the contralateral (non-ischemic) brain hemispheres plausibly because of changes in the pH-dependent amide exchange rate constant (3). APT has previously been used to detect the ischemic penumbra and to provide information complementary to perfusion and diffusion-weighted MRI of ischemic tissues (7). However, despite the successful applications of APT imaging, the robust quantification of isolated amide exchange effects is challenging. The conventional magnetization transfer asymmetry (MTR_{asym}) analysis is sensitive not only to the exchange rate constant but also to various other factors including non-specific magnetization transfer (MT) and asymmetric MT effects, water longitudinal relaxation (T_1), and direct water saturation (RF spillover). Various corrections for these have been proposed. Zhou et al. modeled MTR_{asym} as a superposition of true APT contrast and a baseline shift MTR'_{asym}, which allows changes in APT to be obtained under the assumption that MTR'_{asym} remains unaltered for different physiological perturbations (3). Jin et al. proposed to measure an apparent APT (APT^*), which can be obtained by interpolating measurements at three offset saturating frequencies, as a good approximation of the APT contrast with less contamination from asymmetric MT effects (10). Sun et al. derived MTR'_{asym} numerically and added a correction for tissue relaxation for quantitative pH mapping (11). A number of other methods have also been proposed to isolate the APT contrast from the effects of asymmetric MT, including a two-frequency RF irradiation method (12), saturation with frequency alternating RF irradiations (SAFARI) (13), chemical exchange rotation transfer (CERT) (14), and variable delay multi-pulse (VDMP) methods (15). However, none of these fully correct for RF spillover, MT and T_1 relaxation effects. Recently, Zaiss et al. developed a reciprocal *z*-spectrum analysis which corrects for both MT and spillover effects and incorporates compensation for T_1 (16). Based on this method, we recently described a modified CEST protocol and analysis which combines the three-offset method and the inverse *z*-spectrum analysis to obtain an approximately pure exchange rate weighted contrast (17,18). By implementing such an analysis in APT imaging studies in rodent and human brain tumors (17,19), we have shown

that previously reported APT imaging contrasts obtained using MTR_{asym} and APT* in cancer studies were contaminated by T_1 and/or MT effects. A similar conclusion was also achieved recently in an independent study using a different approach (20). Such findings raise concerns as to whether T_1 and MT effects may strongly contaminate APT data in other applications. This is a fundamental question that must be answered to interpret APT imaging contrast in stroke studies properly.

APT reflects the amide-water exchange effect downfield (to high frequency) from water, but in addition there may be nuclear Overhauser enhancements (NOEs) in the upfield (to low frequency) region of a *z*-spectrum, and these have also been used in the assessment of stroke (10). NOEs can be an additional source of error when using asymmetry-based methods to assess amide effects, but they also may provide additional information. NOEs are believed to originate from mobile proteins, lipids and restricted metabolites through cross relaxation (21–25). Therefore, NOEs also have potential for assessing changes in composition in biological tissues (24). However, NOE imaging in stroke has not been studied comprehensively before, and it is of interest to investigate how NOEs change after stroke occurs, which may provide supplemental information to existing imaging protocols. Note that NOE measurements are also affected by the competing effects mentioned above, yet previous reports have not considered corresponding corrections. Ignoring the influence of such factors may result in ambiguous imaging contrast and make it difficult to interpret NOE measurements.

Here we quantify APT and NOE effects in a rat model of ischemic stroke by extending our previous approach (17,18) and using the reciprocal *z*-spectrum analysis in combination with spline functions to interpolate measurements made at seven offset frequencies. By correcting for RF spillover, MT, and T_1 effects, more robust and isolated measurements of APT and NOE contrasts were obtained. This study may therefore help better understand the contrast mechanisms of APT and NOE imaging in ischemic stroke.

Materials and methods

Quantification of APT and NOE

When a coupled two-pool system such as the free water pool and the amide proton pool (resonance offset frequency Ω = 3.6 ppm) reaches steady-state under a continuous wave (CW) irradiation, the *z*-spectrum values at offsets Ω and $-\Omega$ are given by (16,26)

$$Z(\Omega)=\frac{S(\Omega)}{S_0}=\frac{R_{1a}\cos^2\theta}{R_{eff}+R_{ex}};Z(-\Omega)=\frac{S(-\Omega)}{S_0}=\frac{R_{1a}\cos^2\theta}{R_{eff}} \quad [1]$$

$$R_{eff}=R_{1a}cos^2\theta+R_{2a}sin^2\theta \quad [2]$$

$$R_{ex}=k_{ab}\frac{\omega_1^2}{\omega_1^2+k_{ba}(k_{ba}+R_{2b})} \quad [3]$$

where $\theta=\tan^{-1}(\omega_1/\Omega)$, ω_1 is the irradiation amplitude, k_{ab} and k_{ba} are the exchange rate constants from water to amide proton and the reverse, respectively, R_{1a} and R_{2a} are the longitudinal and transverse relaxation rate constants of water, respectively, and R_{2b} is the transverse relaxation rate constant of amide protons. R_{eff} corresponds to the effective relaxation rate constant in the rotating frame without exchange, and R_{ex} is the exchange-dependent relaxation rate constant (17,18). The magnetization transfer asymmetry (MTR_{asym}) is defined as $MTR_{asym}(\Omega) = Z_{ref}(\Omega) - Z_{lab}(\Omega)$ where the reference scan $Z_{ref}(\Omega) = Z(-\Omega)$ and the label scan $Z_{lab}(\Omega) = Z(\Omega)$ (3). Based on Eq. [1]

$$\mathrm{MTR}_{\mathrm{asym}}(\Omega)=cos^2\theta\frac{R_{\mathrm{ex}}R_{\mathrm{la}}}{R_{\mathrm{eff}}(R_{\mathrm{eff}}+R_{\mathrm{ex}})} \quad [4]$$

Zaiss et al. developed an inverse *z*-spectrum analysis to explain the non-linear interaction of multiple effects (16,18), and defined the apparent exchange dependent relaxation (AREX) as $AREX(\Omega) = (1/Z_{lab}(\Omega) - 1/Z_{ref}(\Omega))\cdot R_{1a}$,so

$$\mathrm{AREX}(\Omega)=\frac{R_{\mathrm{ex}}}{\cos^2\theta}=k_{\mathrm{ab}}\frac{\omega_1^2}{\omega_1^2+k_{\mathrm{ba}}\cdot(k_{\mathrm{ba}}+R_{2\mathrm{b}})}\cdot\frac{1}{cos^2\theta} \quad [5]$$

The term $\cos^2\theta$ is almost 1 (>0.99) for applications at high field strength (e.g. 9.4T) with RF power $B_1 < 2$ μT, and in this case, $AREX(\Omega)$ is expected to increase with ω_1 and to approach k_{ab} when ω_1 is large enough ($\omega_1^2 \gg k_{ba}\cdot(k_{ba}+R_{2b})$, i.e. full saturation).

The advantage of the approach of Zaiss et al. is that T_1 and symmetric MT effects do not contribute to AREX. The theory behind this requires an extension of Eq. [2] to incorporate the relaxation contribution from MT, namely $R_{\mathrm{eff}}=R_{\mathrm{la}}\cos^2\theta+R_{2a}sin^2\theta+R_{\mathrm{ex}}^{\mathrm{MT}}$ (18,27). Exact knowledge of $R_{\mathrm{ex}}^{\mathrm{MT}}$ is then not required. However, in biological tissues, $Z(-\Omega)$ is contaminated by asymmetric MT and NOE effects and is no longer described well by Eq. [1] and thus cannot fulfill the requirement of the reference scan.

The three-offset method proposed by Jin et al. provides an alternative reference scan by interpolating data from two frequencies: for example, Z^*_{ref} (3.6 ppm) = [Z(3.0 ppm) + Z(4.2 ppm)]/2 (10). Then

$$\mathrm{APT}^*=Z_{\mathrm{ref}}^*(3.6\mathrm{ppm})-Z_{\mathrm{lab}}(3.6\mathrm{ppm}) \quad [6]$$

When the amide peak is narrow or far away from the water resonance, Z^*_{ref} can be a good approximation to Z_{ref} (10). Similarly, for quantification of the NOE peak at −3.5 ppm, Z^*_{ref} (−3.5 ppm) = [Z(−5.0 ppm) + Z(−2.0 ppm)]/2, and

$$\mathrm{NOE}^*=Z_{\mathrm{ref}}^*(-3.5\mathrm{ppm})-Z_{\mathrm{lab}}(-3.5\mathrm{ppm}) \quad [7]$$

In the current study, the inverse *z*-spectrum analysis is combined with this three-offset method to better assess APT and NOE changes in vivo, namely

$$\mathrm{AREX}^{*}(\mathrm{APT}) = \left(\frac{1}{Z_{\mathrm{lab}}(3.6\mathrm{ppm})} - \frac{1}{Z^{*}_{\mathrm{ref}}(3.6\mathrm{ppm})} \right) \cdot R_1 \quad [8]$$

$$\mathrm{AREX}^{*}(\mathrm{NOE}) = \left(\frac{1}{Z_{\mathrm{lab}}(-3.5\mathrm{ppm})} - \frac{1}{Z^{*}_{\mathrm{ref}}(-3.5\mathrm{ppm})} \right) \cdot R_1 \quad [9]$$

where R_1 (= $1/T_1$) reflects the observed longitudinal relaxation rate constant of water. Eqs. [8] and [9] benefit from both the removal of spillover and T_1 corrections in the inverse *z*-spectrum analysis and the minimization of asymmetric MT effects by the three-offset approximation, and hence provide an improved approach for assessing APT and NOE in biological tissues.

Animal model

The study was approved by the Institutional Animal Care and Use Committee at Vanderbilt University. MR images were acquired on a 9.4 T Varian 21-cm-bore horizontal imaging system using a 38 mm RF Litzcage Coil (Doty Scientific Inc., Columbia, SC, USA) for both transmission and reception. Six spontaneously hypertensive male rats weighing between 275 and 300 gram were scanned using various pulse sequences for half an hour (baseline images), after which the middle cerebral artery was occluded via the intraluminal suture method (middle cerebral artery occlusion model (MCAO)) as previously described (28). Specifically, a 0.37 mm diameter silicon-coated 4–0 nylon suture (Doccol Corporation, Redlands, CA) was routed into the internal carotid artery on the right side and advanced until it occluded the MCA at a depth of 18–20 mm. Rats were then imaged with the same multimodal sequences every half-hour from 0.5 h up to 3 h post-MCAO. The same multimodal scanning was repeated one more time at 24 h post occlusion. For all MRI studies, animals were anesthetized with 4% isoflurane for induction and 1% to 2% for maintenance. The rat rectal temperature was maintained at ~ 37 °C using a warm-air feedback system. A group of three healthy rats which underwent the same MRI procedures without stroke were used as controls.

In vivo imaging

Scout images were obtained using a fast spin echo multi-slice pulse sequence, with FOV = 40 × 40 (mm), 40 axial slices, 0.5 mm thickness, no gap, TR = 4 s, effective TE = 41 ms, echo train length = 8, matrix size = 128 × 128. After the location was verified, a single axial slice with a thickness of 2 mm was positioned around the Bregma region. The remaining MRI images were acquired with a single-shot spin-echo echo-planar sequence with a triple reference method (29) to reduce ghosting artifacts (FOV=34 × 34 mm, matrix size = 64 × 64, bandwidth = 250 kHz). MRI acquisitions included maps of R_2 (transverse relaxation rate constant), quantitative MT (qMT), diffusion, APT and NOE imaging with a total acquisition time near 30 min. R_2 was measured using four different echo times ranging from 28 ms to 80 ms. Quantitative MT used a selective inversion recovery (SIR) sequence to obtain the pool size ratio (PSR) of the macromolecular MT pool and the observed water longitudinal relaxation rate constant R_1 simultaneously (30,31). Specifically, a 1-ms 180° hard pulse

inverted only the water pool and the subsequent longitudinal recovery was characterized by a bi-exponential curve using 16 inversion times ((ms) 4, 5, 6, 8, 10, 12, 15, 20, 50, 200, 500, 800, 1000, 2000, 4000, 6000). A saturation pulse train was used to speed up acquisition (32). Five parameters were fit from the bi-exponential fit, i.e. R_{1f} (the longitudinal relaxation rate constant of the free water pool), S_f (the efficiency of the 180° inversion pulse on the free water pool), M_f (magnetization of free water before the inversion pulse), k_{mf} (the MT exchange rate constant between macromolecular and free water pools) and PSR. The observed water longitudinal relaxation rate constant R_1 was derived from those five parameters. Note that the free water pool R_{1f} is different from the observed R_1. R_1 is affected by the MT process, while the free water pool R_{1f} represents the intrinsic longitudinal relaxation rate constant. Apparent diffusion coefficients (*ADC*) were measured using a conventional pulsed gradient spin echo (PGSE) sequence with gradients applied simultaneously on three axes (gradient duration = 5 ms, separation = 12 ms, five b-values between 0 and 1000 s/mm^2). APT images were acquired with CW irradiation pulses at six B_1 ((μT) 0.8, 1, 1.2, 1.4, 1.6, 1.8) and eight offsets ((ppm) 2.7, 3, 3.3, 3.6, 3.9, 4.2, 4.5, 300). The saturation pulse duration was 5 s, TR/TE = 7s/28ms. For NOE imaging, the offsets (ppm) were −5.75, −5, −4.25, −3.5, −2.75, −2, −1.25, 300 with B_1 (μT) at 0.2, 0.4, 0.6, 0.8, 1, 1.2.

Data analysis

All data analyses were performed using Matlab (Mathworks, Natick, MA). All images were smoothed by a 2 × 2 filter, and then the brain was manually outlined for pixel-by-pixel fitting. R_2 and *ADC* were measured by fitting the signal decays to mono-exponential functions of echo time and b-value, respectively ($S=S_0e^{-TE*R2}$ and $S=S_0e^{-b*ADC}$). PSR and R_1 were derived simultaneously from the fitting of the signal intensities as a bi-exponential function of inversion time (30,31). For APT imaging (APT* and AREX*(APT)), the seven signals between 2.7 ppm and 4.5 ppm were first normalized by the corresponding control scan (offset = 300 ppm) at each B_1 and then interpolated to nineteen points (Z_{lab}, red squares in Figure 1a) with an interval of 0.1 ppm using a spline function. Instead of the linear interpolation used as a reference by Jin et al. (10), Z^*_{ref} were obtained from a spline interpolation of the four points at (ppm) 2.7, 3, 4.2, and 4.5 (black asterisks in Figure 1a). Spline interpolation may provide slightly better estimation of the baseline than the linear interpolation. To account for possible slight B_0 inhomogeneities, the offset which showed the largest difference between Z^*_{ref} and Z_{lab} was regarded as 3.6 ppm in Eqs. [6] and [8]. By such a means, the effects of small B_0 inhomogeneities were corrected without taking extra scanning time, which was important for this multi-parametric time course study. Note that if SNR is not sufficient, APT* and NOE* may be overestimated. However, since SNR (mean(signal)/std(noise)) was around 400 for the control scan at 300 ppm in this study, it is appropriate to use such a method for fast B_0 correction. The same method was also used for NOE imaging with corresponding offsets. Figure 1 illustrates an example of how Z^*_{ref} and Z_{lab} were obtained based on a representative partial *z*-spectrum of a healthy rat brain. Further analyses were performed on regions of interest (ROI) which were manually selected by reference to the R_1 map at the 3 h time point and applied to all other parametric maps. Figure 2 shows an example of the ROIs drawn on a representative rat brain image. Both hemispheres of the three healthy control rats were taken into consideration, and results are

given as mean ± s.d. (n=6) where applicable. Significances of differences between pre- and post-MCAO in either hemisphere of the ischemic rat brain were estimated using the Wilcoxon rank-sum test.

Results

Multi-parametric maps

Figure 2 shows the multi-parametric MRI maps obtained at each time point. −0.5 h represents the baseline time point before MCAO. In agreement with several previous studies, there are visible changes in several MR parameters immediately after stroke, which evolve over time.

Time courses of R_2, ADC, PSR, and R_1

Figure 3 summarizes the temporal evolution of the average values of R_2*ADC*, PSR, and R_1 in the ROIs prescribed. Consistent with previous reports, R_2 had an initial increase after the onset of ischemia, which has been explained as a blood-oxygen-level-dependent (BOLD) effect (7,33,34). The measured *ADC* had a significant decrease (30%) within 0.5 h after the onset of ischemia, also as reported previously (35–37). R_1 decreased early and continued to drop with similar time course to *ADC*, consistent with earlier reports (38). The PSR stayed around 10% and then dropped to ~ 7% at the 24 h time point, which is in good agreement with a previous qMT study using a different method and analysis (38). The decrease of PSR at the 24 h time point may be related to the breakdown of cell membranes (39) or other macromolecular degradation and the increased water content (38). The measured R_1 in the contralateral hemisphere showed a small but statistically significant increase ($P < 0.01$) from 0.54 ± 0.01 Hz to 0.56 ± 0.01 Hz after the onset of ischemia, but it was not much different from that of healthy controls, which suggests that R_1 in the contralateral hemisphere does not change over time.

APT as a function of the saturation amplitude B_1

Figure 4 shows the change of APT* and AREX*(APT) with different irradiation-powers (B_1) at each time point. APT* in the pre-ischemic rat brain dropped from 2.9% to 1.7% when B_1 increased from 1 μT to 1.8 μT, which is in good agreement with values reported previously (10). During ischemia, the difference of APT* between the contralateral and ischemic hemispheres was about 1%. Consistent with equation [5], AREX*(APT) increased with B_1. The ischemic contrasts were 0.86 ± 0.46% and 2.48 ± 1.00% s^{-1} for APT*(1.8 μT) and AREX*(APT, 1.8 μT) at the 1 h time point, respectively. The corresponding contrast-noise-ratios were 2.43 and 3.21 for APT*(1.8 μT) and AREX*(APT, 1.8 μT). Thus, AREX*(APT) showed greater ischemic contrast than APT* ($P < 0.01$).

NOE as a function of the saturation amplitude B_1

Figure 5 shows the change of NOE* and AREX*(NOE) with the irradiation-power B_1 at each time point. The pre-ischemic NOE* increased up to a maximum at B_1 = 0.6 μT and then dropped with B_1, which is consistent with the previous literature (10). At the 0.5 h time point, the ischemic hemisphere had a larger NOE* than the contralateral hemisphere. However, this difference decreased over time and there was almost no difference at 2.5 h.

Conversely, the magnitude of NOE* in the contralateral hemisphere was higher than that of the ischemic hemisphere at 24 h. Consistent with the theory, AREX*(NOE) increased with B_1 and reached a plateau at around B_1 = 0.8 μT for the pre-ischemic rat brain. The difference of AREX*(NOE) between the contralateral and ischemic hemispheres changed over time.

Time courses of APT and NOE

Based on the measured data and Eq. [5], the values of AREX*(APT, 1.8 μT) and AREX*(NOE, 1.2 μT) seem to yield a good estimation of the exchange rate constants k_{ab} from water to the amide proton and NOE pools, respectively. The temporal evolution of AREX*(APT, 1.8 μT) and AREX*(NOE, 1.2 μT) then provide information about changes in these exchange rate constants. Figure 6 summarizes the temporal variations of APT*(1.8 μT), AREX*(APT, 1.8 μT), NOE*(1.2 μT), and AREX*(NOE, 1.2 μT). The ratio of AREX*(APT, 1.8 μT) between the contralateral and ischemic hemispheres was about 2.38:1 during acute ischemia and increased to 2.84:1 at 24 h. NOE*(1.2 μT) in the ischemic region showed a statistically significant increase ($P < 0.01$) from 2.9 ± 0.6% to 4.9 ± 1.1% after the onset of ischemia and remained almost constant for three hours. Interestingly, the magnitude of NOE*(1.2 μT) in the contralateral hemisphere also had a gradual increase over time and there was almost no difference between the contralateral and ischemic hemispheres after 2.5 h from the onset of ischemia. As for the healthy controls, NOE*(1.2 μT) stayed reasonably constant. Similar to NOE*(1.2 μT), AREX*(NOE, 1.2 μT) also increased gradually in the contralateral (non-ischemic) hemisphere. In the ischemic hemisphere, AREX*(NOE, 1.2 μT) increased immediately after the onset of ischemia but dropped over time.

Discussion

The decrease of *ADC* with acute ischemia has been well documented for a considerable time (35), but the biologic mechanisms responsible for the change remain not fully understood. Several factors have been proposed to explain the *ADC* change. Cellular swelling, for example, may increase the fraction of the intracellular space, which is believed to have a lower *ADC* than the extracellular space (40). Cell swelling may also result in an increased extracellular tortuosity and drop in the effective extracellular diffusion rate (41,42). The intracellular *ADC* has also been reported to decrease and correlate with energy failure (43,44). The reduced R_1 in the ischemic hemisphere at the 24 h time point may be ascribed to water accumulation (38,45), but the early decrease may be evoked by other biologic mechanisms (46,47) because the water content has been reported to be almost constant during the first three hours after the onset of ischemia (38). A 7% decrease of R_1 was previously reported at 9.4 T during initial minutes of ischemia and was attributed to the cessation of blood flow (48). The variation of measured R_1 values over time in the contralateral hemisphere was small but statistically significant ($P < 0.01$), likely a measurement artefact due to the imperfection of the inversion pulse power. The shimming and power calibration were not readjusted after the surgery in order to save time, so the hard inversion pulse may result in some bias in estimates of R_1 and PSR, as suggested by previous numerical simulations (32). The variation of R_1 was only 4%, so its effect on the

quantification of AREX*(APT) and AREX*(NOE) was minor and hence ignored in this study.

The three-offset method has been used earlier to quantify the APT and NOE contrasts in tumor (17) and stroke models (10,18). However, it should be noted that there are two main potential sources of error in APT* and NOE*. First, a high saturation power broadens both APT and NOE peaks, leading to underestimation of APT* and NOE* (10). Meanwhile, with increasing irradiation power, the saturation transfer efficiency reaches a maximum while spillover and MT effects continue to increase (49,50), which can lead to decreased APT* and NOE* contrasts. Thus, the decreased APT* with B_1 (> 0.8 μT) could be attributed to both the increased spillover/MT effects and the increased error of the three-offset method. Second, the exchanging protons of the tissues range from about 1 to 6 ppm and the exchange-relayed NOEs from 0 to −5 ppm. Both APT and NOE peaks may experience interference from neighboring resonances, such as amine protons at 2 and 3 ppm (1,51). Moreover, the effect of these protons on APT/NOE peaks may change during ischemia. Using a pulsed saturation method, Zaiss et al. (18) observed that both APT* and AREX*(APT) decreased after reaching a maximum at the same irradiation power. The decrease of AREX*(APT) was tentatively explained by possible contaminations of the reference scan from nearby amine protons. In this study, a CW irradiation with a narrow bandwidth was used to minimize effects of nearby exchanging protons. Consequentially, AREX*(APT) increased with B_1 and showed no trend to decrease. The increase of AREX*(APT) is consistent with spillover and MT effects having been corrected. However, since AREX*(APT) cannot fully avoid the contaminations from other protons and the inaccuracy of the three-offset method at high saturation powers, AREX*(APT) is still an approximation of the exchange-dependent relaxation rate constant.

Our previous study (17) found out that APT* in tumors was higher than that in normal tissues, but after T_1 correction, AREX*(APT) in tumors was found not significantly different from that in normal tissues. An independent study using a different approach reported similar results (20). This raises the possible concern that previously reported APT imaging studies in stroke may also be contaminated by T_1 or MT effects. Our current study shows that, with a similar data analysis approach, the RF spillover, MT and T_1 corrected APT contrast AREX*(APT) was even more pronounced than using the conventional three-offset estimate. The corrections for RF spillover, MT and T_1 contaminations thus contribute differently in tumor and stroke.

The AREX theory is based on a two-pool model, but in biological tissues water can exist in multiple spaces (e.g., intracellular space, extravascular space and vascular space) with different R_1 in each space and different rates of exchange between them. To the best of our knowledge, there has not been any theory put forward that considers CEST effects in the context of more realistic models of biological tissues. To simplify the model, some appropriate approximations may be made. Because the saturation pulses are long (several seconds) compared to typical intracellular exchange lifetimes (~ 600 ms) (52,53), we assume that water molecules exchange between different compartments and equilibrium is reached between different spaces. If so, the integrated water signal from all spaces can be approximately regarded as a single pool. Under this assumption, though different spaces

have their own R_1, the overall observed (averaged) R_1 of the whole tissue is suitable for the T_1 correction in this simplified "two-pool" system. As mentioned above, the cessation of blood flow may cause the overall observed R_1 to decrease upon acute cerebral ischemia. Though this R_1 change is irrelevant to chemical exchange, it would lead to a change of CEST contrast: R_1 decreases, $Z^*_{\mathrm{ref}} - Z_{\mathrm{lab}}$ increases (54). This APT* contrast change is not related to chemical exchange, so it is necessary to perform the T_1 correction to obtain the true APT contrast.

In this study, variations of NOE* and AREX*(NOE) contrasts in both the contralateral and ischemic hemispheres were observed. NOE*(1.2 μT) provided almost no contrast between the contralateral and ischemic hemispheres after 2.5 h from the onset of ischemia, which is consistent with previous observations by Jin et al. (10). Zhou et al. observed unchanged NOE peaks during acute ischemia and even early postmortem using water exchange spectroscopy (3).Though Jin et al. (10) did not report the time course of NOE*, their results implicitly showed that the NOE*(1.25 μT) increased in either hemisphere when compared to that of the pre-ischemic rat brain. The mean NOE*(1.25 μT) for three healthy and four ischemic rats (after 4 h post-MCAO) was about 3.7% as shown in Figure 6 of Ref. (10). Based on Figure 8 of Ref. (10), the mean NOE*(1.25 μT) for seven ischemic rats (after 4 h post-MCAO) was about 4.5%. The contralateral hemispheres had similar NOE*(1.25 μT) with the ischemic hemispheres after 4 h post-MCAO, so the NOE*(1.25 μT) for the contralateral hemispheres after 4 h post-MCAO was larger than that of the healthy rat brains. Our time course study showed this change more clearly. The explanation of the variation of NOE contrast after the onset of ischemia is unclear, so it will need to be further investigated in future studies. These results indicate that dynamic NOE imaging with multiple time points may provide additional information about stroke progression.

Conclusions

The time courses of APT*, AREX*(APT), NOE* and AREX*(NOE) at multiple irradiation powers were measured in normal and ischemic rat brains, along with several conventional MR parameters R_1, R_2, PSR and *ADC*. Consistent with the inverse metric of the *z*-spectrum revealed by Zaiss et al. (16), AREX*(APT) and AREX*(NOE) were less influenced by B_1 and other confounding effects than APT* and NOE*. Compared with APT*, AREX*(APT) provided greater ischemic contrast. For the first time, we report that NOE* and AREX*(NOE) were observed to increase gradually over time in contralateral hemispheres to the site of injury. Our results may help better understand the contrast mechanisms of APT and NOE imaging in ischemic stroke, and also establish a framework for future stroke measurements using CEST imaging with spillover-, MT- and T_1-corrections.

Acknowledgements

This study was supported by NIH K25CA168936, R01CA109106, R01CA173593, R01EB000214, P50CA128323, R01EB017767 and R21EB017873. The authors thank Ms. Zou Yue for assistance in animal surgeries.

Abbreviations

CEST	chemical exchange saturation transfer
MT	magnetization transfer
APT	amide proton transfer
NOE	nuclear Overhauser enhancement
AREX	apparent exchange dependent relaxation
PSR	pool size ratio of macromolecular pool to free water pool in qMT
ADC	apparent diffusion coefficient

References

1. van Zijl PC, Yadav NN. Chemical exchange saturation transfer (CEST): what is in a name and what isn't? Magn. Reson. Med. 2011; 65(4):927–948. [PubMed: 21337419]
2. Ward KM, Aletras AH, Balaban RS. A new class of contrast agents for MRI based on proton chemical exchange dependent saturation transfer (CEST). J. Magn. Reson. 2000; 143(1):79–87. [PubMed: 10698648]
3. Zhou J, Payen JF, Wilson DA, Traystman RJ, van Zijl PC. Using the amide proton signals of intracellular proteins and peptides to detect pH effects in MRI. Nat. Med. 2003; 9(8):1085–1090. [PubMed: 12872167]
4. Jokivarsi KT, Grohn HI, Grohn OH, Kauppinen RA. Proton transfer ratio, lactate, and intracellular pH in acute cerebral ischemia. Magn. Reson. Med. 2007; 57(4):647–653. [PubMed: 17390356]
5. Jones CK, Schlosser MJ, van Zijl PC, Pomper MG, Golay X, Zhou J. Amide proton transfer imaging of human brain tumors at 3T. Magn. Reson. Med. 2006; 56(3):585–592. [PubMed: 16892186]
6. Sun PZ, Zhou J, Huang J, van Zijl P. Simplified quantitative description of amide proton transfer (APT) imaging during acute ischemia. Magn. Reson. Med. 2007; 57(2):405–410. [PubMed: 17260362]
7. Sun PZ, Zhou J, Sun W, Huang J, van Zijl PC. Detection of the ischemic penumbra using pH-weighted MRI. J. Cereb. Blood Flow Metab. 2007; 27(6):1129–1136. [PubMed: 17133226]
8. Zhou J, Lal B, Wilson DA, Laterra J, van Zijl PC. Amide proton transfer (APT) contrast for imaging of brain tumors. Magn. Reson. Med. 2003; 50(6):1120–1126. [PubMed: 14648559]
9. Zhou J, Tryggestad E, Wen Z, Lal B, Zhou T, Grossman R, Wang S, Yan K, Fu DX, Ford E, Tyler B, Blakeley J, Laterra J, van Zijl PC. Differentiation between glioma and radiation necrosis using molecular magnetic resonance imaging of endogenous proteins and peptides. Nat. Med. 2011; 17(1):130–134. [PubMed: 21170048]
10. Jin T, Wang P, Zong X, Kim SG. MR imaging of the amide-proton transfer effect and the pH-insensitive nuclear overhauser effect at 9.4 T. Magn. Reson. Med. 2013; 69(3):760–770. [PubMed: 22577042]
11. Sun PZ, Wang E, Cheung JS. Imaging acute ischemic tissue acidosis with pH-sensitive endogenous amide proton transfer (APT) MRI--correction of tissue relaxation and concomitant RF irradiation effects toward mapping quantitative cerebral tissue pH. Neuroimage. 2012; 60(1):1–6. [PubMed: 22178815]
12. Lee JS, Regatte RR, Jerschow A. Isolating chemical exchange saturation transfer contrast from magnetization transfer asymmetry under two-frequency rf irradiation. J. Magn. Reson. 2012; 215:56–63. [PubMed: 22237631]
13. Scheidegger R, Vinogradov E, Alsop DC. Amide proton transfer imaging with improved robustness to magnetic field inhomogeneity and magnetization transfer asymmetry using saturation with frequency alternating RF irradiation. Magn. Reson. Med. 2011; 66(5):1275–1285. [PubMed: 21608029]

14. Zu Z, Janve VA, Li K, Does MD, Gore JC, Gochberg DF. Multi-angle ratiometric approach to measure chemical exchange in amide proton transfer imaging. Magn. Reson. Med. 2012; 68(3): 711–719. [PubMed: 22161770]
15. Xu J, Yadav NN, Bar-Shir A, Jones CK, Chan KW, Zhang J, Walczak P, McMahon MT, van Zijl PC. Variable delay multi-pulse train for fast chemical exchange saturation transfer and relayed-nuclear overhauser enhancement MRI. Magn. Reson. Med. 2014; 71(5):1798–1812. [PubMed: 23813483]
16. Zaiss M, Bachert P. Exchange-dependent relaxation in the rotating frame for slow and intermediate exchange -- modeling off-resonant spin-lock and chemical exchange saturation transfer. NMR Biomed. 2013; 26(5):507–518. [PubMed: 23281186]
17. Xu J, Zaiss M, Zu Z, Li H, Xie J, Gochberg DF, Bachert P, Gore JC. On the origins of chemical exchange saturation transfer (CEST) contrast in tumors at 9.4 T. NMR Biomed. 2014; 27(4):406–416. [PubMed: 24474497]
18. Zaiss M, Xu J, Goerke S, Khan IS, Singer RJ, Gore JC, Gochberg DF, Bachert P. Inverse Z-spectrum analysis for spillover-, MT-, and T1 -corrected steady-state pulsed CEST-MRI--application to pH-weighted MRI of acute stroke. NMR Biomed. 2014; 27(3):240–252. [PubMed: 24395553]
19. Zaiss, M.; Windschuh, J.; Meissner, J.; Paech, D.; Radbruch, A.; Bachert, P. Inverse Z-spectrum analysis for clean NOE and amide CEST-MRI - application to human glioma; Proceedings 22nd Scientific Meeting ISMRM; Milan, Italy. 2014. p. 0766
20. Scheidegger R, Wong ET, Alsop DC. Contributors to contrast between glioma and brain tissue in chemical exchange saturation transfer sensitive imaging at 3Tesla. Neuroimage. 2014; 99:256–268. [PubMed: 24857712]
21. Swanson SD. Protein mediated magnetic coupling between lactate and water protons. J. Magn. Reson. 1998; 135(1):248–255. [PubMed: 9799702]
22. Ling W, Regatte RR, Navon G, Jerschow A. Assessment of glycosaminoglycan concentration in vivo by chemical exchange-dependent saturation transfer (gagCEST). Proc. Natl. Acad. Sci. U. S. A. 2008; 105(7):2266–2270. [PubMed: 18268341]
23. van Zijl PC, Zhou J, Mori N, Payen JF, Wilson D, Mori S. Mechanism of magnetization transfer during on-resonance water saturation. A new approach to detect mobile proteins, peptides, and lipids. Magn. Reson. Med. 2003; 49(3):440–449. [PubMed: 12594746]
24. Jones CK, Huang A, Xu J, Edden RA, Schar M, Hua J, Oskolkov N, Zaca D, Zhou J, McMahon MT, Pillai JJ, van Zijl PC. Nuclear Overhauser enhancement (NOE) imaging in the human brain at 7T. Neuroimage. 2013; 77:114–124. [PubMed: 23567889]
25. Zaiss M, Kunz P, Goerke S, Radbruch A, Bachert P. MR imaging of protein folding in vitro employing Nuclear-Overhauser-mediated saturation transfer. NMR Biomed. 2013; 26(12):1815–1822. [PubMed: 24115020]
26. Zaiss M, Bachert P. Chemical exchange saturation transfer (CEST) and MR Z-spectroscopy in vivo: a review of theoretical approaches and methods. Phys. Med. Biol. 2013; 58(22):R221–R269. [PubMed: 24201125]
27. Trott O, Palmer AG 3rd. Theoretical study of R(1rho) rotating-frame and R2 free-precession relaxation in the presence of n-site chemical exchange. J. Magn. Reson. 2004; 170(1):104–112. [PubMed: 15324763]
28. Liu K, Mori S, Takahashi HK, Tomono Y, Wake H, Kanke T, Sato Y, Hiraga N, Adachi N, Yoshino T, Nishibori M. Anti-high mobility group box 1 monoclonal antibody ameliorates brain infarction induced by transient ischemia in rats. FASEB J. 2007; 21(14):3904–3916. [PubMed: 17628015]
29. Hu X, Le TH. Artifact reduction in EPI with phase-encoded reference scan. Magn. Reson. Med. 1996; 36(1):166–171. [PubMed: 8795036]
30. Gochberg DF, Gore JC. Quantitative imaging of magnetization transfer using an inversion recovery sequence. Magn. Reson. Med. 2003; 49(3):501–505. [PubMed: 12594753]
31. Li K, Zu Z, Xu J, Janve VA, Gore JC, Does MD, Gochberg DF. Optimized inversion recovery sequences for quantitative T1 and magnetization transfer imaging. Magn. Reson. Med. 2010; 64(2):491–500. [PubMed: 20665793]

32. Xu J, Li K, Zu Z, Li X, Gochberg DF, Gore JC. Quantitative magnetization transfer imaging of rodent glioma using selective inversion recovery. NMR Biomed. 2014; 27(3):253–260. [PubMed: 24338993]
33. van der Toorn A, Verheul HB, Berkelbach van der Sprenkel JW, Tulleken CA, Nicolay K. Changes in metabolites and tissue water status after focal ischemia in cat brain assessed with localized proton MR spectroscopy. Magn. Reson. Med. 1994; 32(6):685–691. [PubMed: 7869889]
34. Grohn OH, Lukkarinen JA, Oja JM, van Zijl PC, Ulatowski JA, Traystman RJ, Kauppinen RA. Noninvasive detection of cerebral hypoperfusion and reversible ischemia from reductions in the magnetic resonance imaging relaxation time, T2. J. Cereb. Blood Flow Metab. 1998; 18(8):911–920. [PubMed: 9701353]
35. Moseley ME, Cohen Y, Mintorovitch J, Chileuitt L, Shimizu H, Kucharczyk J, Wendland MF, Weinstein PR. Early Detection of Regional Cerebral-Ischemia in Cats - Comparison of Diffusion-Weighted and T2-Weighted Mri and Spectroscopy. Magn. Reson. Med. 1990; 14(2):330–346. [PubMed: 2345513]
36. Schlaug G, Siewert B, Benfield A, Edelman RR, Warach S. Time course of the apparent diffusion coefficient (ADC) abnormality in human stroke. Neurology. 1997; 49(1):113–119. [PubMed: 9222178]
37. Carano RA, Li F, Irie K, Helmer KG, Silva MD, Fisher M, Sotak CH. Multispectral analysis of the temporal evolution of cerebral ischemia in the rat brain. J. Magn. Reson. Imaging. 2000; 12(6): 842–858. [PubMed: 11105022]
38. Makela HI, Kettunen MI, Grohn OH, Kauppinen RA. Quantitative T(1rho) and magnetization transfer magnetic resonance imaging of acute cerebral ischemia in the rat. J. Cereb. Blood Flow Metab. 2002; 22(5):547–558. [PubMed: 11973427]
39. Wolff SD, Balaban RS. Magnetization transfer contrast (MTC) and tissue water proton relaxation in vivo. Magn. Reson. Med. 1989; 10(1):135–144. [PubMed: 2547135]
40. van Gelderen P, de Vleeschouwer MH, DesPres D, Pekar J, van Zijl PC, Moonen CT. Water diffusion and acute stroke. Magn. Reson. Med. 1994; 31(2):154–163. [PubMed: 8133751]
41. Sykova E, Svoboda J, Polak J, Chvatal A. Extracellular volume fraction and diffusion characteristics during progressive ischemia and terminal anoxia in the spinal cord of the rat. J. Cereb. Blood Flow Metab. 1994; 14(2):301–311. [PubMed: 8113325]
42. Binder DK, Papadopoulos MC, Haggie PM, Verkman AS. In vivo measurement of brain extracellular space diffusion by cortical surface photobleaching. J. Neurosci. 2004; 24(37):8049–8056. [PubMed: 15371505]
43. Silva MD, Omae T, Helmer KG, Li F, Fisher M, Sotak CH. Separating changes in the intra- and extracellular water apparent diffusion coefficient following focal cerebral ischemia in the rat brain. Magn. Reson. Med. 2002; 48(5):826–837. [PubMed: 12417997]
44. Harkins KD, Galons JP, Divijak JL, Trouard TP. Changes in intracellular water diffusion and energetic metabolism in response to ischemia in perfused C6 rat glioma cells. Magn. Reson. Med. 2011; 66(3):859–867. [PubMed: 21446036]
45. Knight RA, Dereski MO, Helpern JA, Ordidge RJ, Chopp M. Magnetic resonance imaging assessment of evolving focal cerebral ischemia. Comparison with histopathology in rats. Stroke. 1994; 25(6):1252–1261. [PubMed: 8202989]
46. Ewing JR, Jiang Q, Boska M, Zhang ZG, Brown SL, Li GH, Divine GW, Chopp M. T1 and magnetization transfer at 7 Tesla in acute ischemic infarct in the rat. Magn. Reson. Med. 1999; 41(4):696–705. [PubMed: 10332844]
47. Jokivarsi KT, Hiltunen Y, Tuunanen PI, Kauppinen RA, Grohn OH. Correlating tissue outcome with quantitative multiparametric MRI of acute cerebral ischemia in rats. J. Cereb. Blood Flow Metab. 2010; 30(2):415–427. [PubMed: 19904287]
48. Kettunen MI, Grohn OH, Lukkarinen JA, Vainio P, Silvennoinen MJ, Kauppinen RA. Interrelations of T(1) and diffusion of water in acute cerebral ischemia of the rat. Magn. Reson. Med. 2000; 44(6):833–839. [PubMed: 11108619]
49. Sun PZ. Simultaneous determination of labile proton concentration and exchange rate utilizing optimal RF power: Radio frequency power (RFP) dependence of chemical exchange saturation transfer (CEST) MRI. . J. Magn. Reson. 2010; 202(2):155–161. [PubMed: 19926319]

50. Sun PZ, van Zijl PC, Zhou J. Optimization of the irradiation power in chemical exchange dependent saturation transfer experiments. J. Magn. Reson. 2005; 175(2):193–200. [PubMed: 15893487]

51. Zhou JY, van Zijl PCM. Chemical exchange saturation transfer imaging and spectroscopy. Prog. Nucl. Magn. Reson. Spectrosc. 2006; 48(2– 3):109–136.

52. Meier C, Dreher W, Leibfritz D. Diffusion in compartmental systems. II. Diffusion-weighted measurements of rat brain tissue in vivo and postmortem at very large b-values. Magn. Reson. Med. 2003; 50(3):510–514. [PubMed: 12939758]

53. Quirk JD, Bretthorst GL, Duong TQ, Snyder AZ, Springer CS Jr, Ackerman JJ, Neil JJ. Equilibrium water exchange between the intra- and extracellular spaces of mammalian brain. agn. Reson. Med. 2003; 50(3):493–499.

54. Liu G, Song X, Chan KW, McMahon MT. Nuts and bolts of chemical exchange saturation transfer MRI. NMR Biomed. 2013; 26(7):810–828. [PubMed: 23303716]

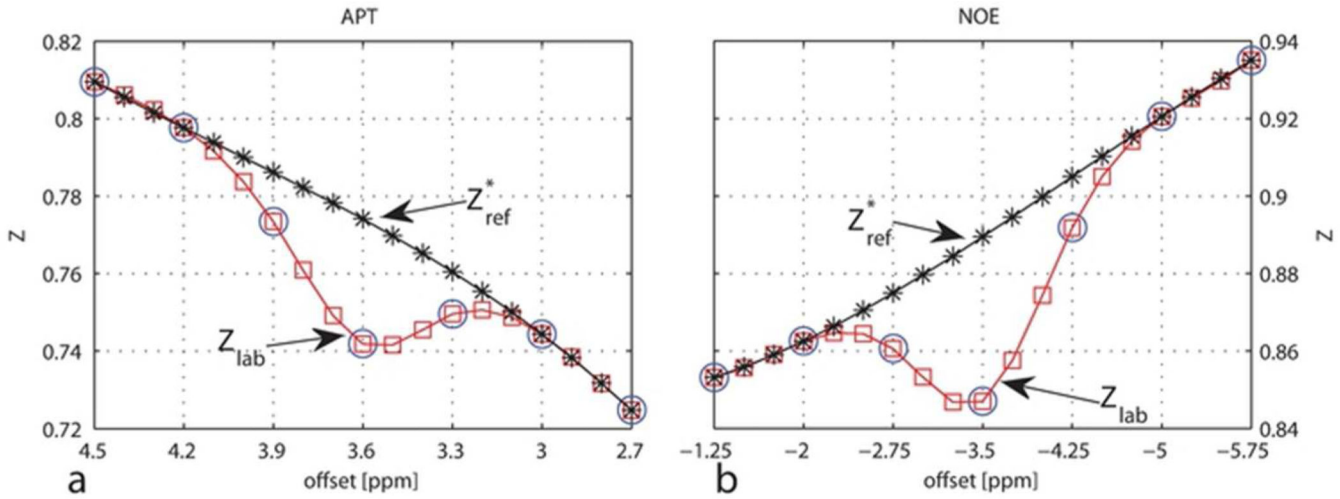

Figure 1.

Illustration of Z^*_{ref} and Z_{lab} for APT (**a**) and NOE (**b**) quantification. The blue circles represent the measured data, from which Z_{lab} (red squares) were obtained using a spline interpolation. The spline interpolation of the points (ppm) 2.7, 3, 4.2, and 4.5 provided Z^*_{ref} (black asterisks) for APT quantification, and the spline interpolation of the points (ppm) −5.75, −5, −2 and −1.25 for NOE quantification.

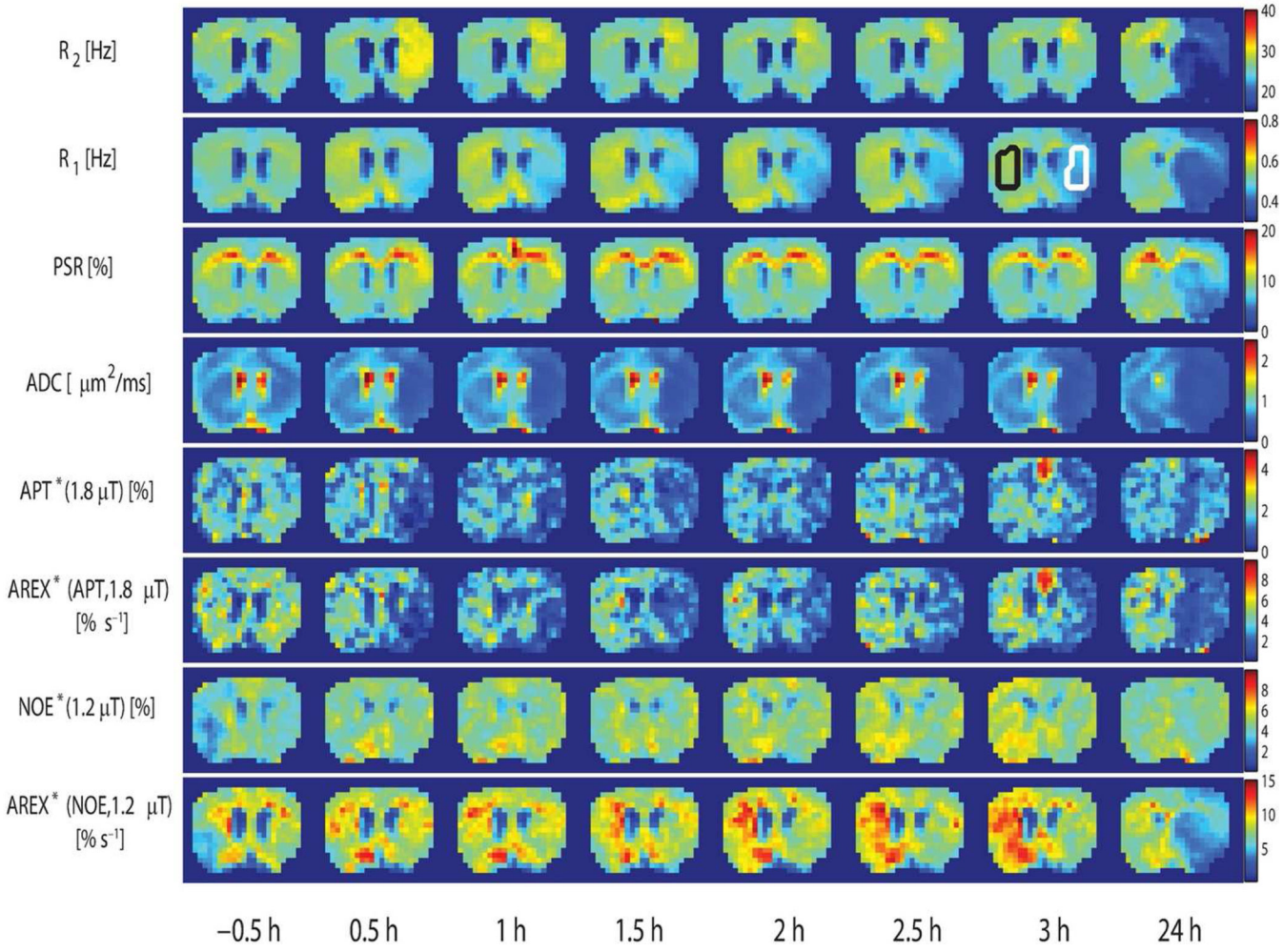

Figure 2.

Temporal evolution of R_2, R_1, PSR, *ADC*, APT*(1.8 μT), AREX*(APT, 1.8 μT), NOE*(1.2 μT), and AREX*(NOE, 1.2 μT) maps acquired from a representative rat. Parametric maps are acquired at time points shown at the bottom. −0.5 h represents the baseline time point before MCAO. The conventional R_2R_1 and *ADC* maps show visible changes immediately after stroke. The R_1 map at 3 h shows the ROIs of the ischemic hemisphere (white) and the contralateral hemisphere (black).

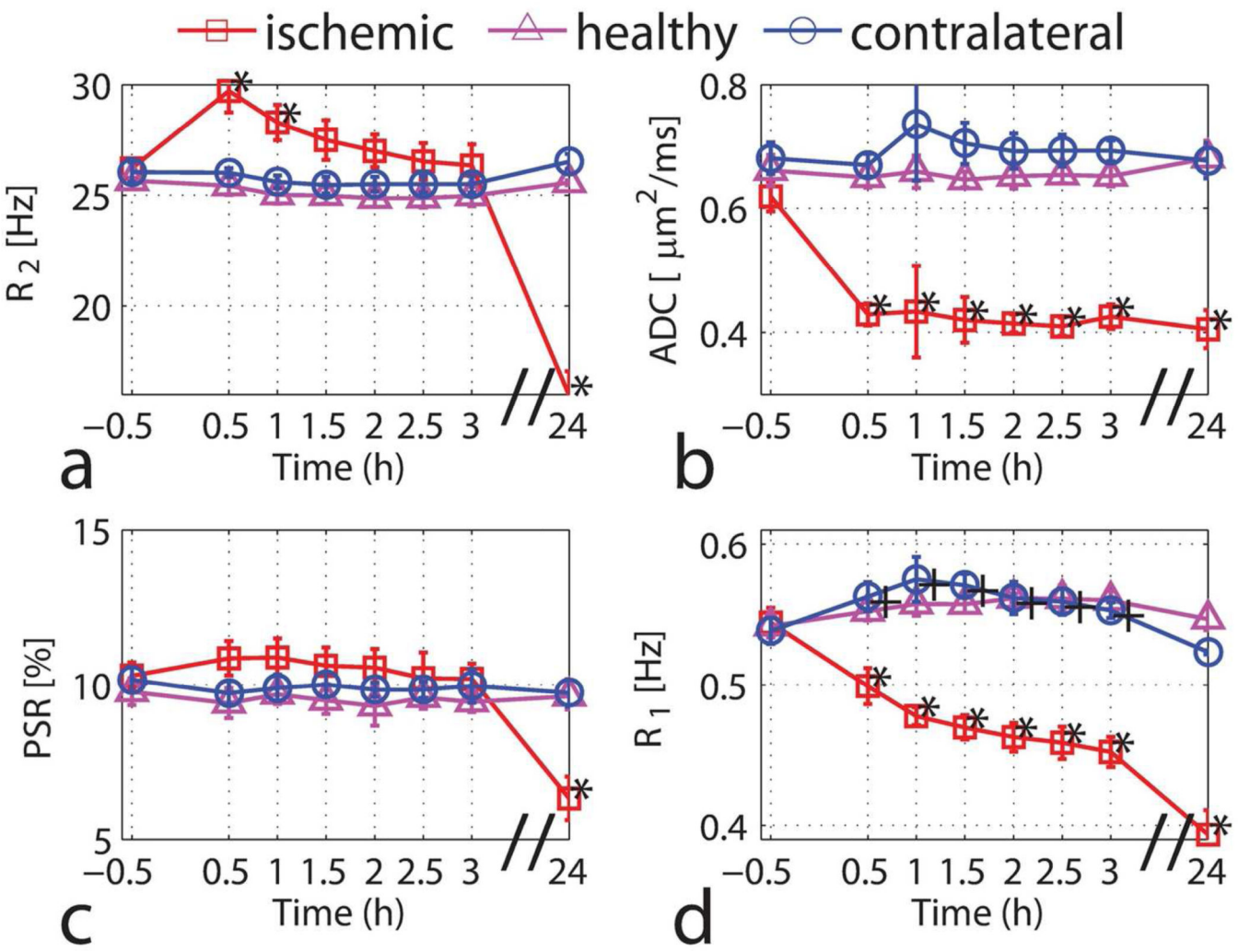

Figure 3.

Time-dependent values of R_2 (**a**), *ADC* (**b**), PSR (**c**) and R_1 (**d**) for the ischemic hemisphere (red squares), the contralateral hemisphere (blue circles) and the healthy controls (magenta triangles). Data are presented as mean ± s.d. (n=6). Statistical significances between pre- and post-MCAO were evaluated using the Wilcoxon rank-sum test (*P<0.01 for the ischemic hemisphere and ^{+}P<0.01 for the contralateral hemisphere).

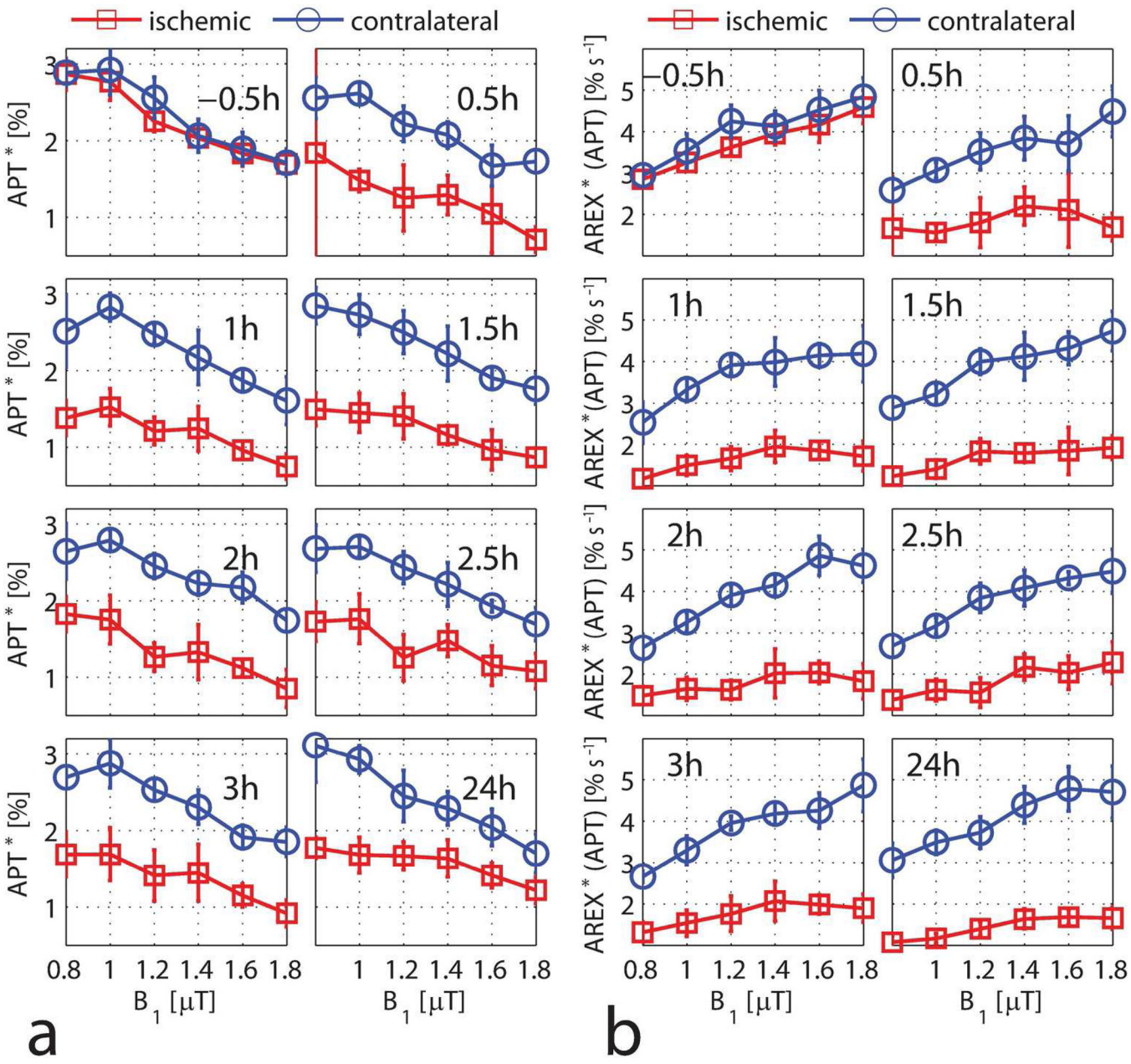

Figure 4.

APT* (**a**) and AREX*(APT) (**b**) as a function of B_1 for the ischemic hemisphere (red squares) and the contralateral hemisphere (blue circles) at each time point. Data are presented as mean ± s.d. (n=6).

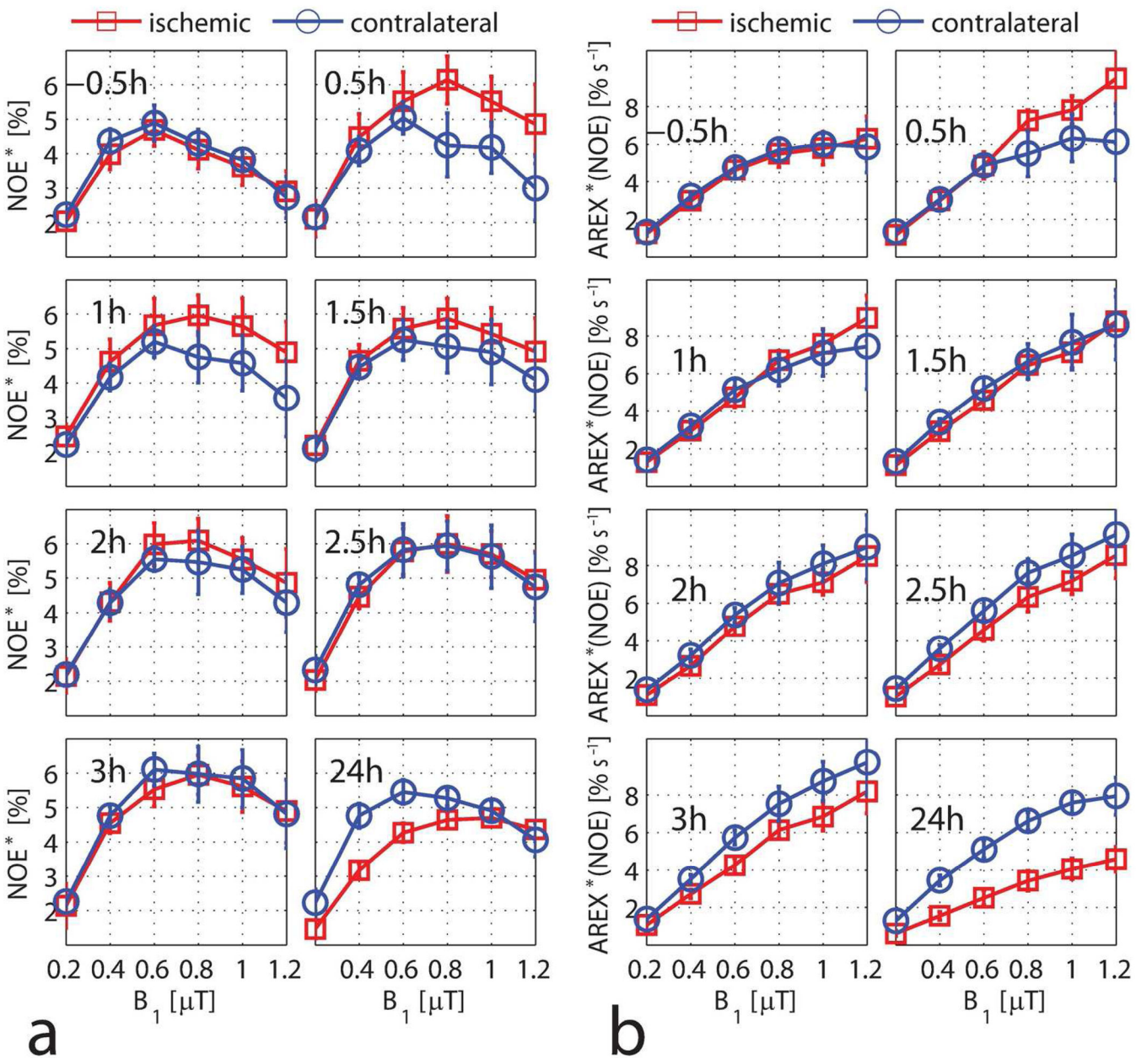

Figure 5.

NOE* (**a**) and AREX*(NOE) (**b**) as a function of B_1 for the ischemic hemisphere (red squares) and the contralateral hemisphere (blue circles) at each time point. Data are presented as mean ± s.d. (n=6).

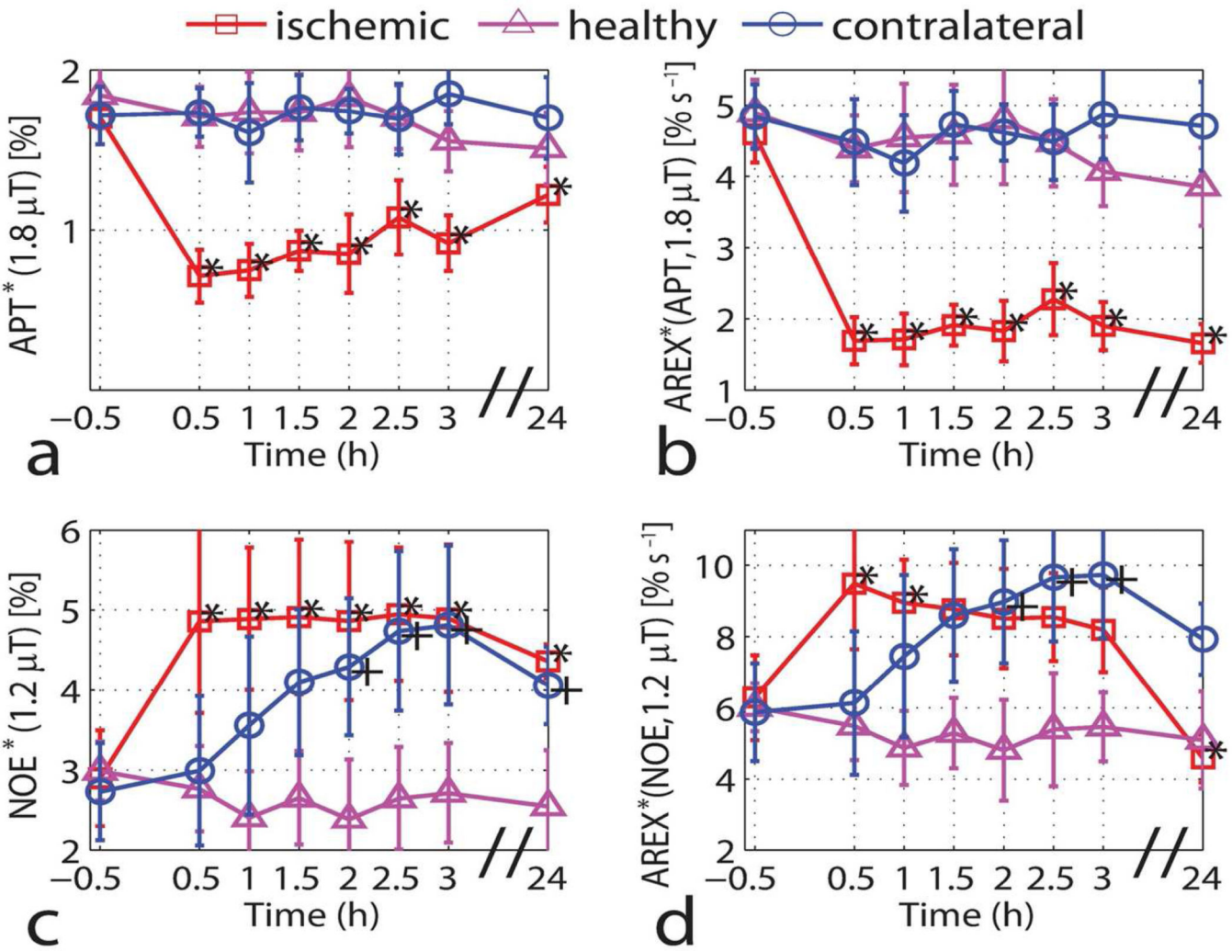

Figure 6.

Time-dependent values of APT*(1.8 μT) (**a**), AREX*(APT, 1.8 μT) (**b**), NOE*(1.2 μT) (**c**) and AREX*(NOE, 1.2 μT) (**d**) for the ischemic hemisphere (red squares), the contralateral hemisphere (blue circles) and the healthy controls (magenta triangles). Data are presented as mean ± s.d. (n=6). Statistical significances between pre- and post-MCAO were evaluated using the Wilcoxon rank-sum test (*P<0.01 for the ischemic hemisphere and ^{+}P<0.01 for the contralateral hemisphere).